^{1}H tunneling transport in crystalline Si of different doping

S. Fabian, S. Kalbitzer,* Ch. Klatt, M. Behar, and Ch. Langpape†
Max-Planck-Institut für Kernphysik, Postfach 103980, D-69029 Heidelberg, Germany
(Received 31 October 1997)

^{1}H has been implanted into crystalline Si at temperatures of $T \sim 40-300$ K in order to study its transport properties. At low implantation energies a major fraction of ^{1}H is mobile; the rest remains trapped up to 500 K. At $T > 200$ K ^{1}H our data complies with the established Arrhenius behavior with an activation energy of $E_a \sim 0.5$ eV and a preexponential factor of $D_0 \sim 10^{-2}$ cm^2/s; at $T < 200$ K, however, the transport follows a power law of $D \sim T^n$ with $n = 5.6$ indicative of a tunneling mechanism. In this range, diffusion is found to be unaffected by the Fermi-level position. Tunneling parameters have been derived and transport paths selected. [S0163-1829(98)03848-X]

I. INTRODUCTION

With the increasing interest in the material properties of Si the influence of impurities on device performance has also been investigated at a steadily rising level. In the past decade, it was found that H can modify the electrical properties of Si by passivating both useful and harmful point defects. After realizing H incorporation to take place in certain fabrication steps, whether intended or not, diffusion measurements have become important.

Already 40 years ago van Wieringen and Warmoltz (vWW) investigated solubility and transport of H in Si using the permeation technique.[1] The narrow temperature range of approximately 1100–1200 K could be represented by the classical Arrhenius law with an activation energy of $E_a = 0.48$ eV and a prefactor of $D_0 = 1 \times 10^{-2}$ cm^2/s indicating interstitial diffusion. During the past two decades measurements of 500–900 K are characterized by large discrepancies in the diffusion coefficients,[2–4] as emphasized by Pearton, Stavola, and Corbett and Pankove and Johnson:[5,6] ^{1}H data by vWW extrapolated to lower temperatures are up to three orders of magnitude larger than, for example, the ^{3}H diffusion coefficients reported by Ichimya and Furuichi.[3]

Later experiments, however, at near room temperature again agree with the extrapolation of the vWW data.[7–9] Moreover, these experiments indicate that H has to be injected under carefully controlled conditions in order to avoid formation of the much less mobile molecule or even larger clusters and trapping by radiation damage.

Recently, first observations of quantum-mechanical motion have been made on ^{1}H transfer between energetically equivalent sites in an impurity complex in Si (Refs. 10 and 11) and on ^{1}H diffusion in the Si matrix at low temperatures.[12] In accord with these latter observations by us calculations by Herrero now predict tunneling of ^{1}H in Si at temperatures below 80 K.[13]

This paper is a quantitative extension of our previous short report.[12] Including the effects of doping on transport we explain the experimental conditions in more detail: (a) injection of ^{1}H into Si with minimum radiation damage; (b) optimization of ^{1}H concentration with respect to H_2 formation and measurability criteria; (c) detection of small changes in ^{1}H depth profiles. The low-temperature results will be discussed in terms of a quantum diffusion mechanism including possible lattice sites and diffusion paths for interstitial ^{1}H.

II. EXPERIMENTAL DETAILS

A. Ion beam facilities

The experiments have been carried out at the Max-Planck-Institut für Kernphysik at Heidelberg by using the 3-MV tandem accelerator together with the low-level background facility for ^{1}H detection.[14,15] A Penning-type ion source has been used for in-line implantation of ^{1}H. The experimental setup is sketched in Fig. 1. The target holder is coupled to a two-stage cryogenerator system in order to provide low target temperatures at UHV conditions better than 10^{-9} mbar. Inside the 4π-cold shield, it is mounted on top of the second refrigerator stage providing 6 sample positions. In addition, a lamp can be used to heat the targets at a rate of 10–15 K/min; temperatures in the range of 40–750 K are accessible.

B. Sample preparation

The samples were prepared from float-zone ⟨111⟩ Si single crystals of low-impurity background with C and O at a level of about 10^{16} at/cm^3. The material is near intrinsic, i.e., lightly doped with 5×10^{13} P/cm^3, except for a few specimens with 1×10^{19} at/cm^3 of B, P, and As.

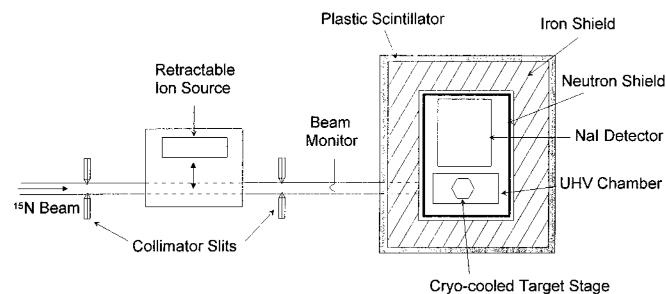

FIG. 1. Scheme of the in-line ion implantation and γ-ray detection system (top view).

 ©1998 The American Physical Society

TABLE I. ^{1}H diffusion data for 100 Ω cm *n*-type Si.

T_A (K)	t_A (sec)	D (cm^2/s)
225	60	8.1×10^{-14}
213	60	2.6×10^{-14}
205	180	2.0×10^{-14}
200	180	1.2×10^{-14}
195	180	5.9×10^{-15}
177	1.8×10^{3}	6.0×10^{-15}
170	1.8×10^{3}	1.4×10^{-15}
158	1.8×10^{3}	1.1×10^{-15}
149	1.8×10^{3}	4.5×10^{-16}
141	1.8×10^{3}	1.0×10^{-15}
134	1.8×10^{3}	3.2×10^{-16}
134	7.2×10^{3}	5.0×10^{-16}
129	1.8×10^{3}	4.0×10^{-16}
129	7.2×10^{3}	3.2×10^{-16}
110	7.2×10^{3}	1.4×10^{-16}
110	2.9×10^{4}	1.3×10^{-16}
89	4.2×10^{4}	3.8×10^{-17}
89	1.1×10^{4}	6.2×10^{-17}
89	2.2×10^{4}	3.6×10^{-17}
89	1.7×10^{5}	2.4×10^{-17}
72	2.6×10^{5}	1.0×10^{-17}
50	6.4×10^{5}	1.7×10^{-18}

The further preparation procedure, including surface passivation, is standard: At room temperature Si samples are etched in a mixture of $HF+HNO_3+CH_3COOH$ saturated with I. By removal of nearly 100 μm reproducible conditions for clean and passivated surfaces are established. After rinsing with deionized water the samples are quickly mounted inside the target chamber and evacuation is started at once.

After cooling the samples to 40 K ^{1}H implantations were performed with a $^{1}H_2^{+}$ beam provided by the in-line Penning ion source at energies between $E_1=0.3-7.5$ keV/amu at current levels of $I=0.1-2$ μA, respectively. Fluences typically ranged between $1-10\times10^{14}$ ^{1}H/cm^2. After implantation the samples were annealed in situ at temperatures in the interval between $T_A=50-225$ K for periods of about $t_A=1-10^4$ minutes, as Table I lists in detail.

C. Depth-profile measurements

The ^{1}H depth profile analysis was performed by using the ^{1}H(^{15}N,$\alpha\gamma$)^{12}C nuclear reaction at the resonance energy of $E=6.385$ MeV with a Lorentzian width of $\Gamma=1.86$ keV. The analyzing currents were about 600 nA of $^{15}N^{2+}$ into a beam spot of approximately 3 mm. The yield curves, recorded in the automatic energy-scanning mode of our accelerator system,[16] were converted to depth profiles by using a specific energy loss of 145 eV/Å for ^{15}N in Si.[17] The detection limit was of the order of 10^{18} ^{1}H/cm^3 with a depth resolution of the order of 1 nm.

The typical depth profile of Fig. 2 consists of two parts: there is a surface peak due to ^{1}H bearing contaminants and, in the deeper region, the implanted ^{1}H profile. The profiles are broadened by characteristic effects:[18,19] (a) Gaussian Doppler broadening due to the zero-point vibration of ^{1}H, by

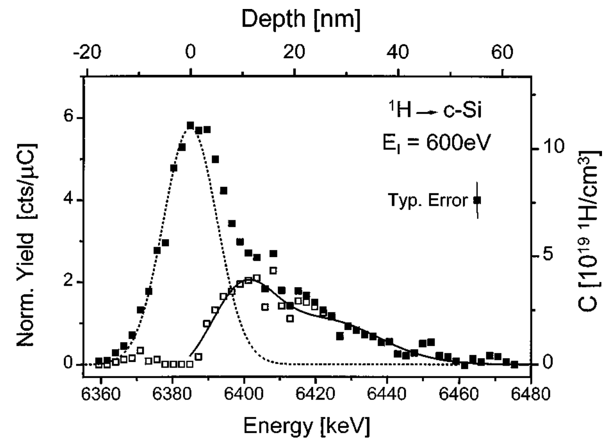

FIG. 2. ^{1}H depth profile obtained by the ^{15}N nuclear-reaction technique. The surface peak (dotted line), due to ^{1}H-bearing contaminants, is subtracted from the measured profile (filled squares) to yield the as-implanted depth distribution of ^{1}H (open squares and full line).

an energy of $\Delta E\sim10$ keV full width at half-maximum equivalent to an uncertainty in depth of $\Delta x\sim7$ nm; (b) channeling of ^{1}H ions during implantation causing penetrating tails; (c) energy-loss straggling of the ^{15}N beam increasing with depth.

We have investigated the influence of the ^{15}N analyzing beam on both ^{1}H components: After exposure to 1×10^{17} ^{15}N/cm^2 the surface component, initially about 1.5 ML (1 ML$=7.8\times10^{14}$ ^{1}H/cm^2 on ⟨111⟩ Si), decreased to 0.1 ML by radiolytic desorption, whereas the as-implanted profiles have not shown any modification during analysis. The question of radiation effects during analysis is nevertheless quite important.[20] As we have observed, a typical exposure to 10^{15} ^{15}N/cm^2 is already sufficient to trap all ^{1}H atoms at their lattice sites. Therefore, we have used each sample for diffusion measurements only once at the temperatures and times summarized in Table I.

As reported previously,[12] we have observed the time evolution of the ^{1}H profiles to agree with regular diffusion kinetics. Thus, we infer that also the results in this paper represent equilibrium conditions.

D. Data analysis

Data evaluation proceeds as follows: First the surface peak, fitted by a Gaussian function, is subtracted from the total spectrum to yield the as-implanted ^{1}H profile. This latter is fitted well by a Pearson-IV function. After annealing the resulting profile changes are evaluated in terms of diffusion coefficients by using the mathematical formalism given by Eqs. (1)–(4) in Appendix A.

These differential equations were solved numerically, using the finite difference method,[21,22] with the boundary conditions: (a) a perfect surface sink, i.e., $C_f(0,t)=0$, and (b) 50% ^{1}H permanently trapped, i.e., $C_f(x,0)=C_t(x,0)=50\%$. The latter assumption is based on the results of Sec. III. Thus, no further trapping and detrapping events had to be taken into account during annealing at lower temperatures. Vacancy depth profiles $C_s(x)$, obtained with the computer code TRIM 91,[17] were used for calculating the initial distribution of trapped ^{1}H.

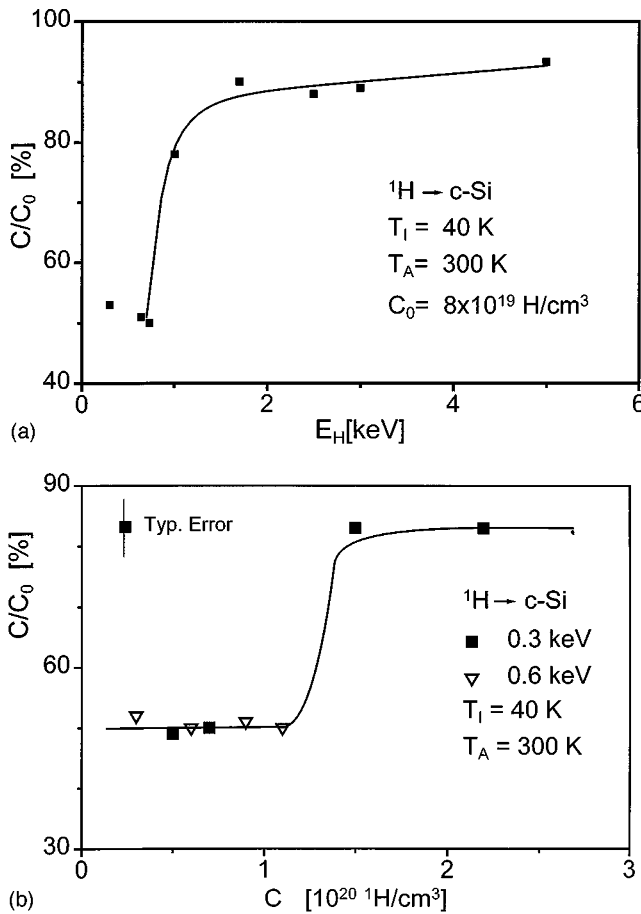

FIG. 3. (a) Fractional retention of low-temperature ^{1}H implants of different energies after warming up to room temperature. (b) ^{1}H fractional retention of low-energy implants as a function of implanted concentration. The solid line is drawn to guide the eye.

III. EXPERIMENTAL RESULTS

In a first experiment, we implanted fluences of $(1-6)\times10^{14}$ ^{1}H/cm^2 at energies of $E_I=0.3-5$ keV corresponding to peak concentrations of $C=8\times10^{19}$ ^{1}H/cm^3. These implantations at 40 K were followed by annealing steps at 300 K for about 10^3 s. The retained fractions of ^{1}H, as shown in Fig. 3(a), exhibit two distinct regions: Above $E_I\sim1$ keV nearly all ^{1}H is trapped, whereas at lower energies up to 50% diffuses out with the complementary fraction remaining inside the implanted region. Thus, $E_I\sim0.6$ keV appears to be close to the optimum condition for diffusion measurements: it leaves a major fraction of ^{1}H free to diffuse with the implanted profile still sufficiently separated from the surface peak. Still lower E_I, further suppressing radiation damage but producing a spectral overlap of bulk and surface components, were found difficult to entangle.

In a second step, we investigated the influence of H concentration on diffusion. H impurity sites, with a capture radius of the order of $r_t\sim1$ nm, tend to form immobile molecules[23] or even higher aggregate centers, e.g., platelets.[24] After implantation at $T_1=40$ K and a subsequent anneal at $T_A=300$ K for a duration of $t_A=10^3$ s the results of Fig. 3(b) were obtained. Evidently, the critical concentration is roughly 10^{20} H/cm^3, above which 100% is rendered immobile and below which about 50% is free to diffuse.

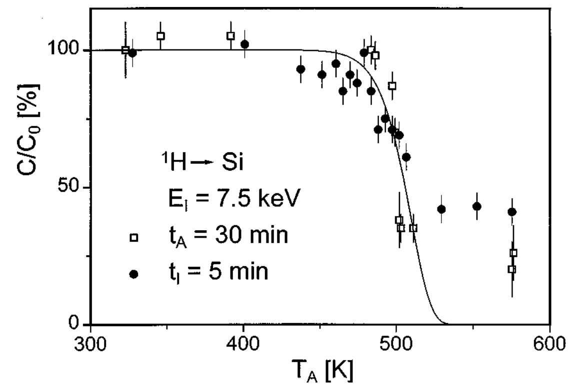

FIG. 4. Isochronal annealing of ^{1}H implants in c-Si at $T_I=300$ K (squares) and at $T_I=T_A$ (dots). In both cases a major fraction of the trapped ^{1}H becomes mobile $T_A\sim500$ K. Note that at $E_I=7.5$ keV nearly 100% of ^{1}H is trapped during implantation, even at $T_I=450$ K.

Therefore $C_H<5\times10^{19}$ H/cm^3 and $E_H=0.6$ keV were chosen as optimum initial conditions.

In order to find out more about the bound fraction we performed two further experiments. First, samples implanted at $T_I=300$ K with 6×10^{14} ^{1}H/cm^2 at $E_I=7.5$ keV exhibit a trapped fraction of nearly 100%, as indicated by Fig. 3(a). The results of isochronal annealing at $T_A=300-600$ K for $t_A=30$ min are displayed in Fig. 4. Up to 475 K there was practically no release, while from 500 K upwards as much as 75% diffused out.

In a second experiment, ^{1}H was implanted and annealed at $T_I=T_A=300-600$ K for $t_A=5$ min. Again, there is complete trapping up to $T_A\sim475$ K, whereas above about 70% diffuse out. These results prove that under both conditions a sufficient number of deep traps exists to render all implanted ^{1}H immobile until detrapping temperatures are reached. In principle, one vacancy could suffice to trap (at least) one ^{1}H. Due to a correlation of the ''end-of-range'' damage with the particle range, correlated trapping is likely to happen at the end of range. Even for a single damage center per implanted impurity remaining theory predicts a noticeable effect as shown by Eq. (A6) in Appendix A.

After having explored the problem of retarded ^{1}H transport in sufficient detail we now turn to the diffusive motion of free ^{1}H. A typical result is shown in Fig. 5, where an initial and diffused ^{1}H depth profile are displayed. Apparently, a fairly good agreement is obtained between experimental and calculated points indicating a diffusion coefficient of $D=1.5\times10^{-17}$ cm^2/s. In this way, all other diffusion coefficients were derived for the investigated temperature interval of $T_A=50-225$ K. The results of additional isothermal annealing steps are summarized in Table I.

Figure 6 is an Arrhenius plot of our present and some recent results by others.[12] The diffusion coefficients can be classified into two groups, if temperature dependence is applied as a criterion. Above 200 K our data points are quite compatible with data reported by Seager, Anderson, and Brice,[7] Tavendale, Williams, and Pearton,[8] Kamiura, Yoneta, and Hashimoto,[9] and extrapolated from the high-temperature regime of vWW.[1] Below 200 K the temperature dependence of the diffusion coefficient, however, is drastically reduced, indicating a different transport mechanism.

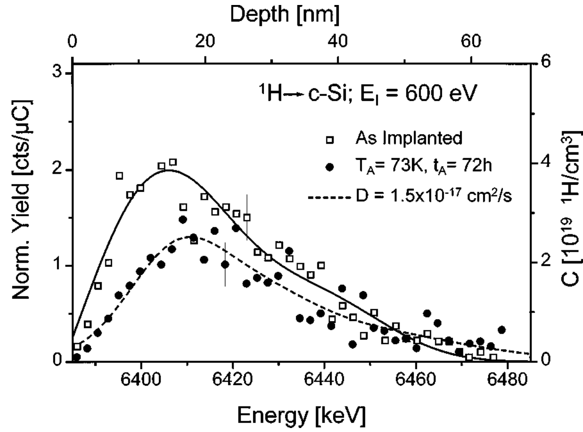

FIG. 5. Full line, Pearson-IV fit to the as-implanted ^{1}H profile; dashed line, numerical calculation of the diffused profile.

Higher dopant concentrations were studied in order to check whether type and/or concentration of doping influence ^{1}H diffusion in c-Si. Highly doped n- and p-type material, with specifications listed in Table II, was implanted with ^{1}H at $T_1=40$ K and annealed at $T_A=130$ K and 170 K for $t_A=1800$ s. The average ^{1}H concentration was kept below the doping levels in order to minimize both H_2 formation and dopant compensation. The results are shown in Fig. 8 together with those from lightly doped Si: no dependence on doping level or type is revealed. In view of the experimental uncertainties, up to about a factor of 3 in the evaluation of $D(T)$ in intrinsic Si, we can neither exclude nor prove the effects of additional ^{1}H trapping in the highly doped specimens within this error bracket.

IV. DISCUSSION

A. High temperature regime

In the Arrhenius plot of Fig. 6 the straight line a is a fit over all data shown in the temperature range of $T>200$ K. The parameters $D_0=(1.1\pm0.2)\times10^{-2}$ cm^2/s and $E_a=(0.49\pm0.01)$ eV are supported by our data points. Surprisingly, these values are very nearly the same as those obtained by vWW in the rather narrow range of 1000–1200 K: $D_0=9\times10^{-3}$ cm^2/s and $E_a=0.48$ eV ($\pm10\%$). The observance of the Arrhenius law indicates a (quasi)classical mechanism with parameters typical for interstitial diffusion between $T=200-1200$ K.

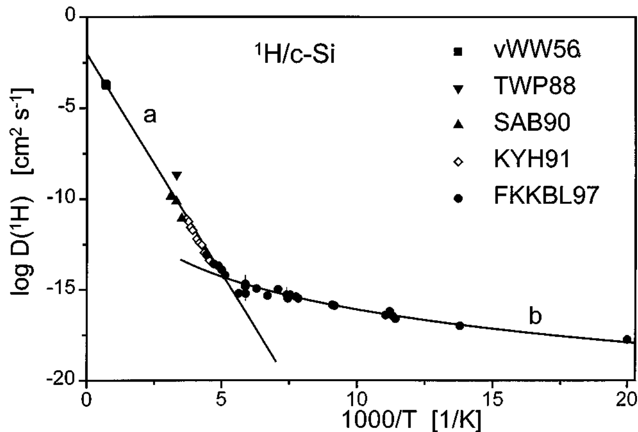

FIG. 6. Arrhenius plot of ^{1}H diffusion data in c-Si. vWW56 is from van Wieringen and Warmoltz (Ref. 1), SAB90 is from Seager, Anderson, and Brice (Ref. 7), TWP88 is from Tavendale, Williams, and Pearton (Ref. 8), KYH91 is from Kamiura, Yoneta, and Hashimoto (Ref. 9), and FKKBL97 is from this work. Note: line a represents classical behavior, while line b indicates tunneling transport.

TABLE II. ^{1}H diffusion coefficients in the tunneling regime for Si of different doping.

	D (cm^2/s)			
T_A (K)	100 Ω cm, n type	10 Ω cm, p type	0.004 Ω cm, n type	0.01 Ω cm, p type
130	3.2×10^{-16}	5.0×10^{-16}		
170	1.4×10^{-15}	2.0×10^{-15}	5.8×10^{-16}	1.6×10^{-15}

The discrepancies with other measurements between 500–900 K,[2–4] where much lower diffusion coefficients were found, can be attributed to trapping effects.[25] In particular, this applies to all previous experiments using ion implantation: Lanford *et al.*[26] and Whitlow *et al.*[27] implanted 10^{16} ^{1}H/cm^2 at 7.5 and 25 keV, respectively, and Fink *et al.*[28] $10^{15}-10^{17}$ ^{1}H/cm^2 at 100 keV. In all these cases diffusion was suppressed, even up to temperatures as high as 500 K.

These results are quite understandable in the light of the effects described in Sec. III: Above a certain kinetic threshold energy, $E_T\sim150$ eV for ^{1}H in Si, damage in the form of Frenkel pairs is created during implantation. This occurs predominantly at the end of the range of the projectile, where nuclear stopping dominates. This effect is clearly demonstrated by calculations of radiation defect generation by swift protons using the $T2D$ routine described by Biersack and Haggmark.[29] Figures 7(a) and 7(b) refer to ^{1}H projectiles of $E_1=7.5$ and 0.6 keV producing, on average, approximately 3.5 and 0.5 vacancies/ion, respectively, for a displacement energy of $E_D=20$ eV. As the results of previous gas retention measurements show,[12] the probability is quite high that each ^{1}H projectile is trapped by one of its self-generated vacancies at the end of its track. Figure 7(c) displays the predictions by Eq. (6) for a certain set of implantation and trap properties.[30] Thus, $p\sim10\%$ per correlated vacancy for $r_0=1$ nm and $r_i=10$ nm, which explains our experimental observation of major fractions of trapped ^{1}H. This effect is largely independent of other implantation events at low dose rates and operates at any implantation energy exceeding the threshold energy E_T. Therefore, a substantial fraction of free ^{1}H can only be observed if the generated lattice damage is reduced to less than 1 vacancy/ion. As demonstrated above, the conditions for free diffusion can only be achieved by a proper choice of implantation energy and concentration.

An analysis of the data of Fig. 4 by use of Eq. (A7) indicates that the initial annealing rate of trapped ^{1}H follows first-order kinetics with a dissociation energy of $E_d=1.6\pm0.1$ eV and a trap depth of $E_b=1.1\pm0.1$ eV, according to Eq. (A5) of Appendix A. With increasing release, retrapping modifies the kinetics. It is interesting to note that ^{1}H diffusion in amorphous silicon is characterized by a similar activation energy of $E_a\sim1.5$ eV;[31,32] saturation of dangling bonds is known to occur, likely in a vacancy in crystalline Si

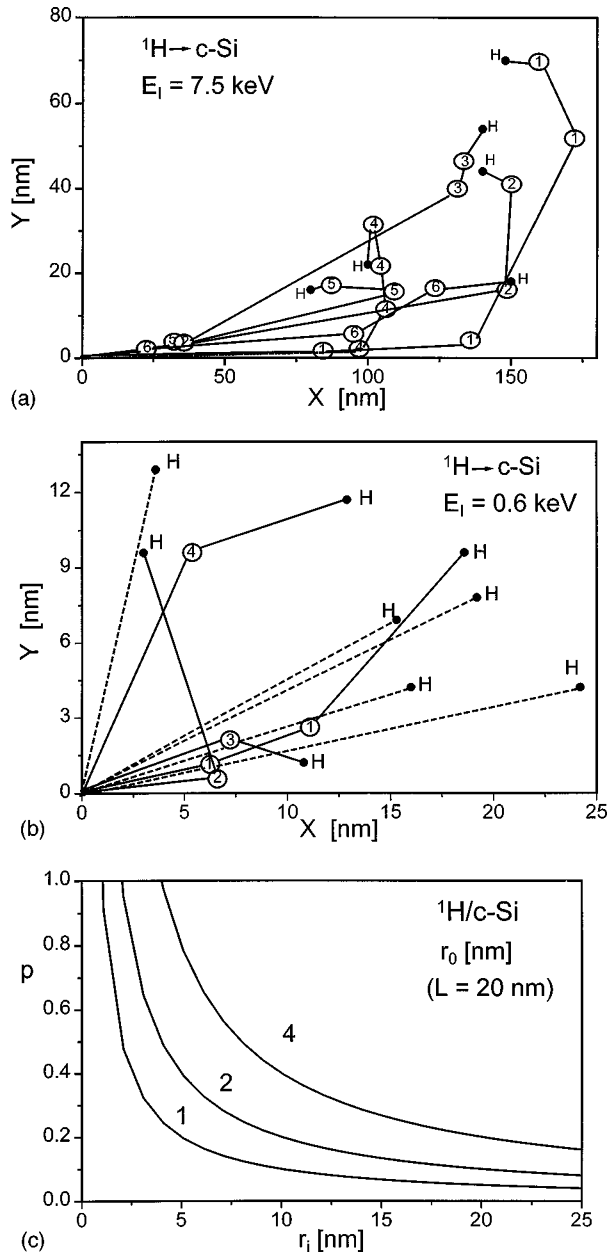

FIG. 7. (a) Six trajectories of ^{1}H ions of 7.5 keV energy in crystalline Si in a 2D projection. The final position of each ^{1}H is shown together with those of the produced vacancies (marked by the respective number). Note: the correlated distances ^{1}H/vacancy are approximately 10–50 nm; the average number of vacancies is 3.5/ion. (b) Seven trajectories of ^{1}H of 0.6 keV energy in crystalline Si in a 2D projection. The final position of each ^{1}H is shown together with those of the produced vacancies (marked by the respective number). Note: the correlated distances ^{1}H/vacancy are approximately 10 nm, average number of vacancies 0.5/ion. (c) Probability p of a diffusing atom to get trapped at a center of capture radius r_0 at distance r_i for a diffusion length of $L=20$ nm.

as well. These experimental figures, however, are considerably below theoretical values of $E_d=2.1$ and 2.4–2.7 eV.[33,34]

B. Low-temperature regime

Below 200 K the temperature dependence of the diffusion coefficient is very weak. If an Arrhenius equation is fitted to

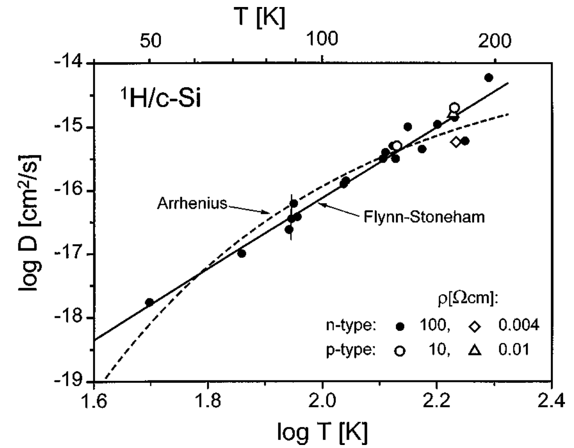

FIG. 8. Double log plot of diffusion coefficients vs temperature; best fit by a power relation $D \propto T^n$ with $n=5.6$ (solid line).

the data of curve b in Fig. 6, the resulting parameters $D_0 = (2\pm1)\times10^{-14}$ cm^2/s and $E_a=43\pm4$ meV are difficult to explain within the framework of classical bulk transport theory. Since no transient effects have been observed so far, i.e., the usual dependence of the diffusion length of $L\propto t^{0.5}$ for thermodynamic equilibrium systems is obeyed,[12] a recombination enhanced mechanism involving electronic carriers[35] can be ruled out as well as any other exhaustible source of additional energy.

A quantum-mechanical tunneling mechanism, however, can explain our experimental data.[12] The theory of thermally activated tunneling (hopping) processes, as formulated by Flynn and Stoneham (FS) is based on Holstein's principle of the small polaron, a particle in an energetically relaxed lattice site.[36,37] It has been applied to the diffusion of light interstitials in fcc and bcc metals. The corresponding expressions take relatively simple forms only for high and low temperatures of $T>\theta_D$ and $T<\theta_D/3$, respectively; the formalism for the latter is given in the section Appendix B.

According to Fig. 8, our low temperature data are fitted well by a straight line with a slope of $n=5.6\pm0.3$. This is in agreement with the FS prediction of $n\sim5-7$ for a two-phonon tunneling process,[38] where one phonon is absorbed for excitation to the coincidence level and reemitted for deexcitation to the neighboring ground state.[39] From the straight line the quantity Ja of Eq. (B7) can be derived, if the coincidence energy of the excited state E_c is known. Figure 9 is an energy scheme of the relevant particle states involved in the diffusion process. For $E_c\sim54(27)$ meV (Ref. 40) we ob-

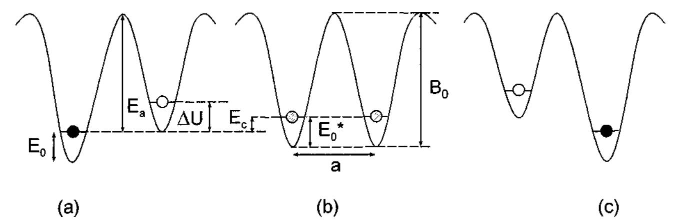

FIG. 9. Thermally assisted tunneling: (a) the ground state of a self-trapped atom in a well, (b) the excited state in a coincidence configuration for tunneling into a neighboring site, and (c) the ground state after the transition. The chosen energy levels are: $E_a=500$, $E_0=100$, $\Delta U=100$, $E_c=50$, $B_0=500$, and $E_0^*=100$ meV.

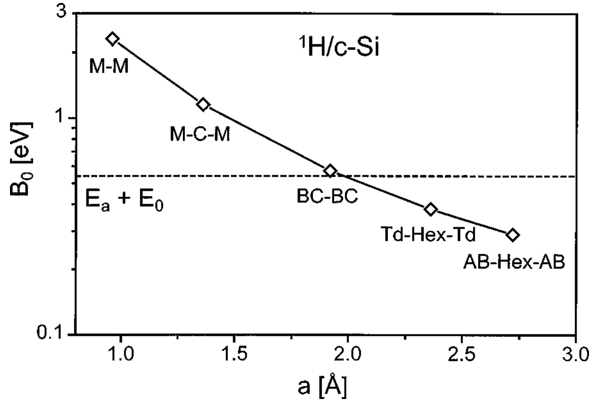

FIG. 10. Potential barriers B_0 correlated with tunneling distances a for a tunneling parameter of $Ja=70$ neV Å; zero-point energy levels E_0^* of ^{1}H in the coincidence state are taken into account.

tain $Ja \sim 70(40)$ neV Å. This value is quite low as compared to $Ja \sim 100$ meV Å for reorientational tunneling in the Si-B-^{1}H complex[10,11] or to $Ja \sim 50$ meV Å for tunnel transport of ^{1}H in bcc transition metals, but it is very roughly in the range observed for fcc metals, e.g., $Ja \sim 0.01-10$ neV Å for ^{1}H/Pd.[41,42] Probably, larger tunnel distances and/or higher tunnel barriers, typical for fcc lattice structures, are also responsible for the small values for the system ^{1}H/Si.

The further analysis of the quantity Ja is carried out by using the tunneling formalism as given by Kehr.[42] The measured value of Ja together with an assumed range of a $\sim 1-3$ Å yields a correlated bandwidth for the tunnel barrier of $B_0 \sim 3-0.3$ eV. As explained in Appendix B, the key tunneling parameter is $\kappa = \gamma a B_0^{1/2} \sim 0.75$ Å eV$^{1/2}$. Kehr treats only the case of negligible zero-point energy of the excited particle, for which the form factor $\gamma = 2/\pi$ is obtained for a sinusoidal tunneling barrier. We obtain $\gamma = 0.52$, if zero-point effects on the tunneling integral are considered. In addition to the statistical error of the measured quantity Ja of $\pm 5\%$, the uncertainty of the expression $5E_c/h\omega_D$ in Eq. (14) by an estimated factor of 2 leads to a systematic error of $\Delta B_0/B_0 \sim \pm 5\%$. Thus, a total error of $\Delta B_0/B_0 \sim \pm 10\%$ has to be accepted in the correlation plot of tunneling barrier versus distance displayed in Fig. 10.

The results of the evaluation of the individual barrier heights for different tunneling distances are listed in Table III. We note that the ratio of zero-point energy/barrier height of the coincidence configuration [see Fig. 9(b)] is very nearly constant for all cases: $E_0^*/B_0 \approx 10\%$. All of these values appear reasonable and also compatible with total energy-surface calculations,[43–46] so that we see no objections against the application of FS theory to the tunneling regime of ^{1}H diffusion in Si.

We now turn to the interesting question of which tunneling path is taken by the interstitial ^{1}H. The lattice positions of six interstitial sites, as described in the literature,[20,46] are shown in Fig. 11. The following criteria have to be satisfied for tunneling transport: (1) occupation of minimum-energy ground states, (2) same ground state for classical and tunneling diffusion, (3) momentum conservation in tunneling transitions, and (4) extended tunneling transport paths through the crystal.

TABLE III. Tunneling paths of interstitial ^{1}H in Si.

Path	a (Å)	B_0 (eV)[a]	E_0^* (meV)
M-M	0.96	2.30	224
M-C-M	1.36	1.15	112
BC-BC AB-AB Hex-Hex C-C	1.92	0.57	56
C-AB-C AB-C-AB C-Hex-C Hex-C-Hex C-BC-C Td-Hex-Td	2.36	0.38	37
AB-Hex-AB AB-BC-AB	2.72	0.29	28

[a]Evaluated from Eq. (B6). Note: $\kappa = \gamma a B_0{}^{1/2} \sim 0.75$ Å eV$^{1/2}$, $\gamma = 0.52$, $E_0^*/B_0 \approx 0.1$.

The first requirement means that transport events have to start from a lattice site of lowest energy, so that its occupation by the diffusing particle is sufficient under thermal equilibrium conditions. In general, classical and quantum-mechanical diffusion must occur from the same ground state. In contrast to classical motion, where the particle can take different directions from the saddle point, quantum-mechanical transfer has to follow a straight path segment. Finally, a complete transport route through the crystal in all three directions is required, i.e., reorientational or one-dimensional (1D) motions have to be ruled out.

From Table III, listing 14 straight diffusion paths characterized by five groups of nearest-neighbor pairs, the selection proceeds by using calculated site energies. This discrimina-

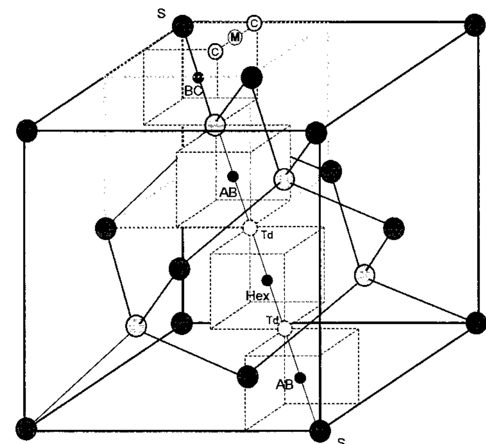

FIG. 11. Lattice sites of interstitial H in a diamondlike lattice: S (substitutional), BC (bond center), AB (antibonding), Hex (hexagonal), M (middle), C (corner), and T_d (tetrahedral).

tion procedure constitutes a very sharp measure for competing sites under thermodynamical equilibrium conditions.

According to several theory groups, the bond-center (BC) site is energetically most favorable.[13,44,45,47] Thus, it is a candidate for tunneling along a straight path to a neighboring BC site at a distance of 1.92 Å. (We note that we previously excluded the straight tunneling path BC-BC on the basis of a too crude estimate of tunneling probability.[12]) Our experimental value of Ja yields a potential height of $B_0 = 0.57$ eV, quite close to the classical value of $B_0 = E_a + E_0 \sim 0.5 + 0.05 = 0.55$ eV, where the estimated zero-point energy of the ground state, $E_0 = 50$ meV, is somewhat uncertain. The proposed classical path BC-C-BC (where C is corner) is characterized by a calculated activation energy of $E_a \sim 0.3$ eV (Ref. 48) to be compared with the measured one of $E_a = 0.5$ eV.[1,7–9] It was recently also proposed for tunneling by Herrero.[13] Since it is not a straight path, it has to be ruled out for direct tunneling transitions because of the violation of momentum conservation.

The middle (M) site was proposed by Corbett *et al.* as the ground state of interstitial ^{1}H;[43] van de Walle found M to be only slightly higher in energy than the BC site and the potential surface in-between flat,[44] so that the particle possibly occupies both places with similar probabilities. As regards energetic conditions, high-temperature transport could proceed along M-C-M over a calculated barrier of only $E_a \sim 0.3$ eV,[43] which, in view of the computational uncertainties, is not too far away from the experimental value of $E_a = 0.5$ eV. According to Fig. 10, however, the correlated tunnel barrier height has to be $B_0 = 1.15$ eV for the distance $a = 1.36$ Å. Since for the same path the potential barriers for jumping over and tunneling through should be roughly the same, the difference between E_a and B_0 is too large as to justify this choice. In addition, M-C-M would be a 1D path only, which is another argument against it.

The straight path M-M, proposed as a tunneling path before in Ref. 12, is characterized by the short distance $a = 0.96$ Å and the correlated barrier height $B_0 = 2.30$ eV, which appears to be too high in view of theoretical estimates by van de Walle.[49] Another problem is seen in the fact that there would be no classical path originating from an M site for the high-temperature regime for reasons given above. If we disregard this two objections, then the only explanation left would be to postulate an energetic degeneracy of M and BC sites with a vanishing barrier in between.[44] In this case, the particle would classically jump along BC-C-BC at high temperatures satisfying the condition of $E_a = 0.5$ eV and tunnel along M-M at low temperatures. We emphasize, however, that the permitted energetic difference of M and BC sites would have to be rather small in order to facilitate an approximately equal population down to temperatures of 50 K, with an energy equivalent of approximately 5 meV.

All other possibilities listed in Table III can be ruled out by the consensus of all theoretical groups, i.e., all these site levels are energetically too high as to be populated. At 100 K, for example, a relative level difference of only 0.1 eV would reduce the respective population of the upper level by a factor of 10^{-5}. Thus, even if the tunneling parameter κ should allow this transition, as possibly in the cases AB-Hex-AB (where AB is antibonding) and Td-Hex-Td,[33,50] there would be no atoms to participate in. Figure 12 visualizes the remaining tunneling paths BC-BC and M-M over several atomic distances together with the classical path BC-C-BC.

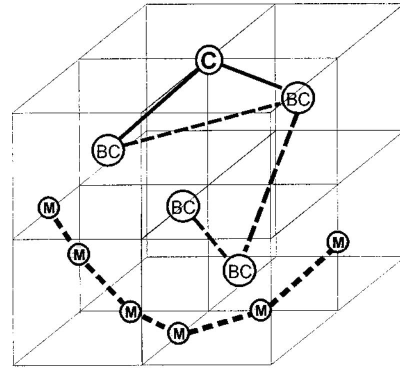

FIG. 12. The two most likely 3D-tunneling paths between interstitial sites of ^{1}H in the Si lattice. The cube length is half the lattice constant of the Si unit cell.

We now turn to the question of the electronic charge of H in Si. H is known to exhibit deep electronic levels in the band gap;[51] drift experiments have convincingly demonstrated the existence of charged H.[5,6,8] Depending on the Fermi-level position it can assume the charge states H^+, H^0, and H^-. Another theory maintains that it constitutes a negative U system with the result that only H^+ and/or H^- states can exist depending on the Fermi-level position.[52,53] Thus, doping effects would cause large changes in the diffusion coefficients, if the diffusion barriers change with the charge state of H. Quite surprisingly, our diffusion coefficients in the tunneling transport regime have not shown any difference between the heavily doped and the nearly intrinsic material. At present, we cannot draw any conclusion other than that the tunneling barriers must be nearly the same, since the differences in the atomic mass due to one or two excess electrons are negligible as regards tunneling probabilities.

Built-in fields, as usually encountered in the near-surface region of semiconductors, would influence both classical and quantum-mechanical motion of charged ^{1}H. As outlined in Appendix B, an electrical field of $F \sim 1$ V/μm would enhance both transport coefficients by about qFa/kT and $4qF\chi^{1/2}/\pi B_0{}^{1/2}$, respectively. For $a \sim 0.1$ nm, $B_0 \sim 1$ eV and $T \sim 300$ K both effects are roughly 0.3%. By using the relation between drift and diffusion lengths, $\lambda = p\delta^2$ with the drift strength parameters $p_{\mathrm{cl}} = qF/kT$ and $p_{\mathrm{qm}} = 4qF\chi^{1/2}/\pi B_0{}^{1/2}$, we find drift and diffusion lengths equal for $\lambda = \delta \sim 30$ nm. Tables I and II indicate typical diffusion lengths of this order. Thus, if these conditions apply, the effect of a superimposed drift on $D(H^+)$ or $D(H^-)$ should be inside our quoted experimental errors.

V. CONCLUSIONS

The low-temperature diffusion of ^{1}H in c-Si can be reconciled with the tunneling theory by Flynn and Stoneham for a two-phonon mechanism. Tunneling transport paths of ^{1}H may be realized between BC-BC sites, which are also believed to be the ground states for classical transport. Tunneling between M-M sites could occur, only if BC and M levels are energetically degenerate and not separated by a barrier.

Tunneling probabilities of ^{1}H have been found independent of the Fermi-level position in c-Si.

ACKNOWLEDGMENTS

Our thanks are due to R. Schwan, who took great care in preparing the samples by mechanical and chemical techniques. M. Behar is a visiting guest from UFRGS, Porto Alegre, Brazil.

APPENDIX A: DIFFUSION AND TRAPPING KINETICS

The differential equations describing particle diffusion in the presence of one type of trapping center read

$$dC_f/dt = Dd^2C_f/dx^2 - \mu C_f + \nu C_t, \quad \text{(A1)}$$

$$dC_t/dt = \mu C_f - \nu C_t, \quad \text{(A2)}$$

where $C_f(x,t)$ and $C_t(x,t)$ are the concentration of free and trapped particles, respectively, and $C = C_f + C_t$ is the total particle concentration; D is the diffusion coefficient, μ and ν are trapping and detrapping rates, respectively, given by the usual relations:

$$\mu = 4\pi r_t D C_S(x), \quad \text{(A3)}$$

$$\nu = \nu_0 \exp(-E_d/kT). \quad \text{(A4)}$$

Here r_t is a trapping radius and $C_S(x)$ the local trap concentration, while ν_0 is the attempt frequency to leave the trap and E_d the corresponding detrapping energy. E_d is the sum of the binding energy E_b and the activation energy E_a, equal to the migration energy in the case of an interstitial diffusor:

$$E_d = E_b + E_a. \quad \text{(A5)}$$

The important process of correlated trapping of the implanted particle and the damage generated by itself at the end of range can be described by the relation[30]

$$p = (r_0/r_i)\mathrm{erfc}[(r_i - r_o)/L)], \quad \text{(A6)}$$

where p is the trapping probability, r_i the distance diffusor trap, r_0 the trap capture radius, and $L = 2(Dt)^{1/2}$ the diffusion length.

The corresponding dissociation energy is readily derived by applying Eqs. (A2) and (A4). If retrapping is negligible, a straightforward integration gives

$$E_d = kT \ln[\ln(C_t/C_0)/\nu_0 t], \quad \text{(A7)}$$

where a vibrational frequency of $\nu_0 \sim 10^{13}\ \mathrm{s}^{-1}$ for ^{1}H seems to be appropriate.

APPENDIX B: MATHEMATICAL FORMALISM FOR TUNNELING TRANSITIONS

The estimation of quantum-mechanical transition rates starts with the assumption of a simple lattice potential. For a sinusoidal potential of the form

$$B(x) = \tfrac{1}{2}B_0[1 + \cos(2\pi x/a)], \quad -a/2 \leq x \leq a/2, \quad \text{(B1)}$$

Kehr derives for the tunneling matrix element[42]

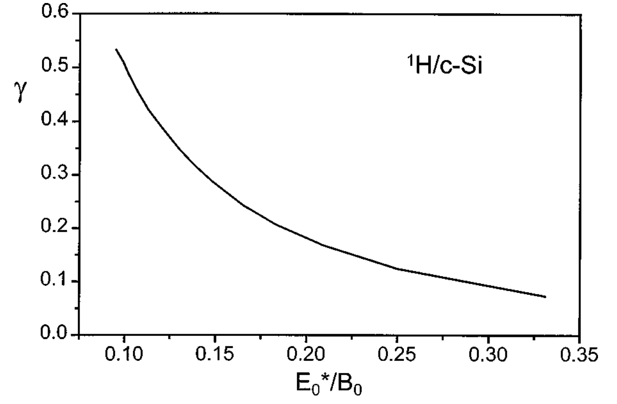

FIG. 13. Form factor for tunneling through a sinusoidal barrier vs ratio of zero-point energy and barrier height of the excited state.

$$J = 8B_0\chi^{-1/4}\exp(-2\chi^{1/2}/\pi),$$

$$\chi = 2ma^2B_0/\hbar^2, \quad \text{(B2)}$$

where B_0 is the barrier height, a the tunneling distance, and m the mass of the diffusor. As depicted in Fig. 9, the zero-point energy E_0^* of ^{1}H in the coincidence configuration of Fig. 9(b) has to be considered unless $E_0^* = \frac{1}{2}\hbar\omega_0^* \ll B_0$. This criterion seems not too well fulfilled in the present case.

The zero-point energy of the excited state is obtained from Eq. (B1) as

$$E_0^* = \tfrac{1}{2}\hbar\omega_0^* = \pi B_0{}^{1/2}/a(2m)^{1/2} = 0.142 B_0{}^{1/2}/a, \quad \text{(B3)}$$

with units of energy in eV and of distance in Å. For example, we obtain for $B_0 = 1$ eV and $a = 1$ Å a zero-point level at $E_0^* = 142$ meV, which is not small. Its effect on the form factor of the tunneling integral is

$$\gamma = \int [B(x)]^{1/2}dx = \int \{\tfrac{1}{2}[1 + \cos(2\pi x/a)]^{1/2}\}dx,$$

$$\text{with } x_0 = \pm a \cos^{-1}(2E_0^*/B_0 - 1)/2\pi \quad \text{(B4)}$$

as upper and lower integration limit, respectively. Figure 13 demonstrates the strong dependence of the form factor γ on the ratio E_0^*/B_0. With our value of $\kappa = 0.75$ Å eV$^{1/2}$ we derive

$$E_0^*/B_0 = \pi\gamma/\kappa(2m)^{1/2} \sim 0.19\gamma, \quad \text{(B5)}$$

which ratio assumes a value of nearly 0.1 for $\gamma = 0.52$ for all cases considered in Table III. Since for a chosen tunneling path of length a γ is uniquely determined by B_0, we have

$$\gamma(B_0) = \kappa/aB_0^{1/2}. \quad \text{(B6)}$$

By plotting both left- and right-hand side of Eq. (B6) versus B_0 we obtain the lines of Fig. 14, where the crossing points determine the barrier heights for each chosen tunneling distance a given by the unrelaxed lattice positions.

The temperature dependence of the diffusion coefficient in the tunneling regime is by a power law reflecting the operating phonon process. For the low-temperature regime of $T < \Theta_D/3$ Flynn and Stoneham specified[37]

$$D = ga^2\Gamma(T),$$

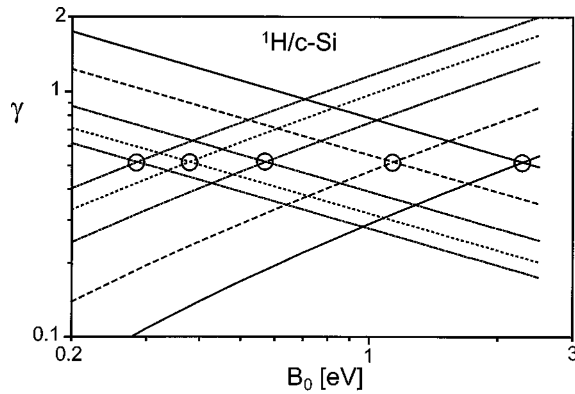

FIG. 14. Graphical determination of the form factor for a sinusoidal potential of different barrier heights including zero-point energy effects. Note that $\gamma=0.52$ for all cases.

$$\Gamma(T)=A(T/\Theta_D)^n,$$

$$A=57\,600\pi\omega_D J^2 E_c^2 \exp(-5E_c/\hbar\omega_D)/(\hbar\omega_D)^4, \quad \text{(B7)}$$

where g is the geometrical factor, a the tunneling distance, Γ the tunneling rate, $\omega_D=k\Theta_D/\hbar$ the Debye frequency, Θ_D the Debye temperature, e.g., $\Theta_D(\mathrm{Si})=640\pm40$ K, E_c the coincidence energy (see Fig. 9), J the tunnel transition matrix element, and n the order of phonon process, e.g., $n=5-7$ for a two-phonon process.[38]

For the purpose of illustration we have chosen a set of typical energy levels in Fig. 9, which may be not too far from the actual conditions for a BC-BC tunnel transition. The influence of an electrical field on the transport coefficients is given by the expressions

$$\eta_{\mathrm{cl}}=qFa/kT, \quad \text{(B8a)}$$

$$\eta_{\mathrm{qm}}=4qF\chi^{1/2}/\pi B_0{}^{1/2}. \quad \text{(B8b)}$$

The quantum-mechanical enhancement η_{qm} amounts to about 0.3% for typical conditions of $a\sim0.1$ nm, $B_0\sim1$ eV, and $F\sim1$ V/μm for ^{1}H in Si; the classical factor η_{cl} would also be about the same at $T\sim300$ K.

By using the relation between drift and diffusion lengths,[54]

$$\lambda=p\delta^2, \quad \text{(B9)}$$

with the the drift-strength parameters

$$p_{\mathrm{cl}}=qF/kT, \quad \text{(B10a)}$$

$$p_{\mathrm{qm}}=4qF\chi^{1/2}/\pi B_0{}^{1/2}, \quad \text{(B10b)}$$

we find drift and diffusion lengths equal for $\delta=1/p$, which may serve to estimate the relative importance of the two transport mechanisms. In the present case we find $1/p\sim30$ nm.

It should be noted, however, that drift causes displacements of concentration profiles, whereas diffusion effects broaden their shapes. Thus, the case of $\lambda\gg\delta$ should be identified easily, whereas the unidentified case of $\lambda\sim\delta$ could lead to a change in D by about $[(\delta+\lambda)/\delta]^2\sim4$.

*Corresponding author. Fax: +49 6221 516-540. Electronic address: S.Kalbitzer@mpi-hd.mpg.de
†Now at SAP, Walldorf, Germany.
[1] A. van Wieringen and N. Warmoltz, Physica (Utrecht) **22**, 849 (1956).
[2] M. Capizzi and A. Mittiga, Appl. Phys. Lett. **50**, 918 (1987).
[3] T. Ichimiya and A. Furuichi, Int. J. Appl. Radiat. Isot. **19**, 573 (1968).
[4] N. M. Johnson and M. D. Moyer, Appl. Phys. Lett. **46**, 787 (1985).
[5] S. Pearton, M. Stavola, and J. Corbett, in *Hydrogen in Crystalline Semiconductors*, Springer Series in Materials Science Vol. 16 (Springer-Verlag, Berlin, 1992).
[6] J. Pankove and N. Johnson, in *Hydrogen in Semiconductors* (Academic, Boston, 1991).
[7] C. H. Seager, R. A. Anderson, and D. K. Brice, J. Appl. Phys. **68**, 3268 (1990).
[8] A. J. Tavendale, A. A. Williams, and S. J. Pearton, in *Defects in Electronic Materials*, edited by M. Stavola, S. J. Pearton, and G. Davies, MRS Symposia Proceedings No. 104 (Materials Research Society, Pittsburgh, 1988), p. 285.
[9] Y. Kamiura, M. Yoneta, and F. Hashimoto, Appl. Phys. Lett. **59**, 3165 (1991).
[10] Y. M. Cheng and M. Stavola, Phys. Rev. Lett. **73**, 3419 (1994).
[11] K. Muro and A. J. Sievers, Phys. Rev. Lett. **57**, 897 (1986).
[12] Ch. Langpape, S. Fabian, Ch. Klatt, and S. Kalbitzer, Appl. Phys. A: Mater. Sci. Process. **64**, 207 (1996).
[13] C. P. Herrero, Phys. Rev. B **55**, 9235 (1997).
[14] H. Damjantschitsch, M. Weiser, G. Heusser, S. Kalbitzer, and H. Mannsperger, Nucl. Instrum. Methods Phys. Res. **218**, 129 (1983).
[15] P. Oberschachtsiek, M. Weiser, and S. Kalbitzer, Nucl. Instrum. Methods Phys. Res. B **56/57**, 1010 (1991).
[16] G. Amsel, E. d'Artemare, and E. Girard, Nucl. Instrum. Methods Phys. Res. **205**, 5 (1983).
[17] J. F. Ziegler, J. P. Biersack, and U. Littmark, in *The Stopping and Ranges of Ions in Solids* (Pergamon, New York, 1975).
[18] B. Hartmann, S. Kalbitzer, and M. Behar, Nucl. Instrum. Methods Phys. Res. B **103**, 494 (1995).
[19] B. Hartmann, S. Kalbitzer, and Ch. Klatt, Nucl. Instrum. Methods Phys. Res. B **113**, 50 (1996).
[20] B. Bech-Nielsen, Phys. Rev. B **37**, 6353 (1988).
[21] J. Crank, in *The Mathematics of Diffusion*, 2nd ed. (Clarendon, Oxford, 1975), p. 137.
[22] J. Kashny and M. Behar, Nucl. Instrum. Methods Phys. Res. B **111**, 51 (1996).
[23] C. H. Seager and R. A. Anderson, Appl. Phys. Lett. **53**, 1181 (1988).
[24] N. M. Johnson, C. Donald, F. A. Ponce, J. Walker, and G. Anderson, Physica B **170**, 3 (1991).
[25] T. Zundel and J Weber, Phys. Rev. B **46**, 2071 (1992).
[26] W. A. Lanford, H. P. Trautvetter, J. F. Ziegler, and J. Keller, Appl. Phys. Lett. **28**, 566 (1976).
[27] H. J. Whitlow, J. Keinonen, M. Hautala, and A. Hautojärvi, Nucl. Instrum. Methods Phys. Res. B **5**, 505 (1984).
[28] D. Fink, J. Krauser, D. Nagengast, T. Almeida Murph, J. Erxmeier, L. Palmetshofer, D. Bräunig, and A. Weidinger, Appl. Phys. A: Mater. Sci. Process. **61**, 381 (1995).

[29] J. P. Biersack and L. G. Haggmark, Nucl. Instrum. Methods **174**, 257 (1980).
[30] G. Dienes and G. Vineyard, *Radiation Effects in Solids* (Interscience, New York, 1957), p. 146.
[31] M. Reinelt, S. Kalbitzer, and G. Müller, J. Non-Cryst. Solids **59/60**, 169 (1983).
[32] J. Kakalios in *Hydrogen in Semiconductors*, edited by J. Pankove and N. Johnson (Academic, Boston, 1991), p. 424.
[33] C. G. van de Walle, Phys. Rev. B **49**, 4579 (1994).
[34] S. K. Estreicher, Mater. Sci. Eng., R. **14**, Nos. 7–8, 319 (1995).
[35] L. Kimerling, Solid-State Electron. **21**, 1391 (1978).
[36] T. Holstein, Ann. Phys. (N.Y.) **8**, 343 (1959).
[37] C. P. Flynn and A. M. Stoneham, Phys. Rev. B **1**, 3966 (1970).
[38] A. M. Stoneham, Collect. Phenom. **2**, 9 (1975).
[39] Y. Fukai and H. Sugimoto, Adv. Phys. **34**, 263 (1985).
[40] G. Dolling and R. A. Dowley, Proc. Phys. Soc. London **88**, 463 (1966).
[41] T. Heumann, in *Diffusion in Metallen*, Werkstoff-Forschung und Technik Vol. 10 (Springer-Verlag, Berlin, 1992), p. 219.
[42] K. Kehr, in *Hydrogen in Metals I*, edited by G. Alefeld and J. Völkl (Springer Verlag, Berlin, 1978), p. 203.
[43] J. W. Corbett, S. N. Sahu, T. S. Shi, and L. C. Snyder, Phys. Lett. A **93**, 303 (1983).
[44] C. G. van de Walle, Y. Bar-Yam, and S. T. Pantelides, Phys. Rev. B **39**, 10 791 (1989).
[45] P. Deak, L. C. Snyder, and J. W. Corbett, Phys. Rev. B **37**, 6887 (1988).
[46] S. Tiansheng, S. N. Sahu, J. W. Corbett, and L. C. Snyder, Sci. Sin. **27**, 98 (1984).
[47] A. D. Marwick in *Hydrogen in Semiconductors*, edited by J. Pankove and N. Johnson (Academic, Boston, 1991), p. 185.
[48] C. P. Herrero and R. Ramirez, Phys. Rev. B **51**, 16 761 (1995).
[49] C. van de Walle (private communication).
[50] A. A. Bonapasta, A. Lapiccirella, N. Tomassini, and M. Capizzi, Europhys. Lett. **7**, 145 (1988).
[51] D. Mathiot, Phys. Rev. B **40**, 5867 (1989).
[52] P. Anderson, Phys. Rev. Lett. **34**, 953 (1975).
[53] N. M. Johnson, C. Herring, and C. G. van de Walle, Phys. Rev. Lett. **73**, 130 (1994).
[54] S. Kalbitzer, in *Proceedings of the Fourth EC Photovoltaic Solar Energy Conference, Stresa*, edited by W. H. Bloss (Reidel, Dordrecht, 1982), p. 1059.